Supplementary Material for

Stabilization and humanization of a single-chain Fv antibody fragment specific for human lymphocyte antigen CD19 by designed point mutations and CDR-grafting onto a human framework

Markus Kügler, Christoph Stein, Michael Schwenkert, Domenica Saul, Lena Vockentanz, Thomas Huber, Svava K. Wetzel, Oliver Scholz, Andreas Plückthun, Annemarie Honegger* and Georg H. Fey

Biochemisches Institut der Universität Zürich
Winterthurerstrasse 190
CH-8057 Zürich
Switzerland

*Corresponding author.
Email address: honegger@bioc.uzh.ch

Present addresses:
M.K, C.S, M.S, D.S, G.F, Institute of Biology, University of Erlangen-Nuremberg, Erwin-Rommel-Strasse 3, D 91058 Erlangen, Germany
S.K.W, O.S, A.P, A.H, Biochemisches Institut der Universität Zürich, Winterthurer-strasse 190, CH-8057 Zürich, Switzerland
L.V, Max-Delbrück-Centrum für Molekulare Medizin, Robert-Rössle-Straße 10, D-13125 Berlin-Buch, Germany
T.H, Novartis Biologics / Protein Design, WSJ-506.3.13, Novartis Pharma AG, CH-4002 Basel

Keywords: antibody engineering; immunoglobulin variable domains; framework 1 structure; scFv fragment; stability

Design of the CDR graft

The AHo numbering scheme (Honegger and Plückthun, 2001b) for immunoglobulin variable domains used throughout this paper has been developed to facilitate the automated comparative analysis of antibody structures, in particular the analysis of sequence-structure relationships in the CDR regions and the analysis of antigen-antibody interactions. In contrast to other numbering schemes for antibody variable domains, such as Kabat (Kabat *et al.*, 1991), Chothia (Chothia and Lesk, 1987; Al-Lazikani *et al.*, 1997) and IMGT (Lefranc *et al.*, 2003), it pays particular attention to the placement of the alignment gaps in CDRs of different lengths in such a way that structurally equivalent residues obtain the same residue numbers. As a result of this analysis of all antibody structures available in the Protein Data Bank (http://www.rcsb.org/pdb/) at the time of the analysis, we compiled tables of average solvent exposure for each residue, involvement in interchain- and interdomain- interactions and differential antigen contact probabilities for distinct antigen binding modes. We differentiate "hapten binding", denoting a binding mode where the antigen inserts deeply into the V_L/V_H interface, "peptide binding", where an elongated groove facilitates the binding of linear epitopes, and "protein binding", where the hapten binding pocket is filled with CDR-H3 residues and a relatively flat binding surface facilitates the binding of structural epitopes. The aim of that study was to provide a solid structural basis for the design of CDR randomization strategies for the human combinatorial antibody library (HuCAL®) (Knappik *et al.*, 2000; Rothe *et al.*, 2008).

Those results of the analysis that are relevant to the design of a CDR-graft (Honegger, 2008) are summarized as color codes in Figure S1. More information can be found on the AAAAA website (http://www.bioc.uzh.ch/antibody/). The average contribution of the different sequence positions to antigen contacts, interchain- (V_L/V_H) and interdomain- (V_L/C_L and V_H/C_H) contacts (Figure S1c) was determined by comparing the solvent accessibility of each residue in the relevant complex to its accessibility in the isolated domain. The color code represents the average reduction in solvent accessibility, from white, residues not involved in the interface in any of the structures analyzed, over shades of yellow and orange, to red for residues fully buried in the interface in all structures analyzed. Projected onto a homology model or structure of an antibody scFv fragment, these antigen contact probabilities offer a more differentiated view of the putative antigen binding site than the CDR definitions of Kabat (Kabat et al., 1991), Chothia (Chothia and Lesk, 1987; Al-Lazikani *et al.*, 1997) and IMGT (Lefranc et al., 2003) (Figure S1b).

In addition to the antigen binding interface, the V_L/V_H interface is also relevant to the successful design of a CDR graft, since residue substitutions in this interface can affect the relative orientation of the two domains and thereby the topography of the antigen binding interface.

The average side chain accessibility (Figure S1d) distinguishes between residues fully buried in the individual domain (yellow), partially exposed (shades of green) or highly exposed, pointing into the solvent from exposed loop regions (blue). The fully buried residues (yellow) that make up the domain core can be divided into three groups: The packing of the upper core residues supports the CDRs, residue substitutions in this group have a high probability of affecting the CDR conformations and indirectly affect antigen affinity. The central core (blue) is a group of highly conserved residues that shield the upper core from the high diversity of the lower core. Packing of the lower core residues (green) is fairly conserved in V_L domains, while in V_H domains it is conserved within individual germline family, but varies between germline families and structural subtypes.

In the region of CDR-H2, this clean separation between upper core, central core and lower core breaks down. In CDR graft from a non-human antibody to the closest human homolog, this normally does not make any problems, since the packing of the lower core is conserved between the most closely related germline families of different species. It becomes a problem in grafts to a divergent V_H framework subtype (Honegger and Plückthun, 2001a; Honegger, 2008). The packing interactions between the upper core residues derived from the CDR donor and the lower core residues derived from the acceptor framework have to be carefully analyzed and optimized to avoid excessive destabilization or alteration of the CDR-H2 conformation or take-off angle, leading to a major loss of antigen binding affinity. However, subtle differences in backbone conformation, side-chain orientations and core packing interactions cannot always be fully compensated by mutational change of a few contact residues, leaving some residual strain. In grafts from an intrinsically weak antibody to a highly stable one, this residual strain is masked by the stability gain imparted by the more stable acceptor framework. However, the direct comparison of grafts to acceptor frameworks of different structural subtypes (Willuda *et al.*, 1999; Honegger *et al.*, 2008) and grafts from an intrinsically stable framework, such as the mutationally stabilized 4G7-mut, show that if the stability of a graft fails to reflect the superior stability of a highly stable acceptor framework, it can be due to a structural mismatch between CDR donor and acceptor

framework. A graft to a more closely related, though intrinsically somewhat less stable framework may yield superior results and should be considered as an alternative.

With the exception of the mutation of Leu H12 to Asp, which was introduced solely to improve the folding efficiency of the V_H domain, as discussed for 4G7-mut, all mutations in 4G5-graft aimed at retaining the antigen affinity of the CDR donor while avoiding destabilizing interactions with divergent residues in the acceptor framework. Such destabilizing interactions would either reduce the thermodynamic stability of the graft, or change the loop conformations and reduce the antigen affinity.

Further analysis of the equilibrium denaturation data

In systems that conform to a two-state equilibrium of unfolding the stability $\Delta G_{(H2O)}$ of a molecule can be derived from a linear extrapolation to [D]=0 of ΔG, calculated from the equilibrium constant, as a function denaturant concentration.

The tryptophan fluorescence emission spectrum was used to monitor the unfolding of the scFv (Figure S2, Table ST1). While the fluorescence intensity Y is linearly dependent on the fraction of molecules unfolded, the signal-to-noise ratio of this measurement is very poor, since it is highly sensitive to light scattering due to aggregation and to errors in the protein concentration (Figure S3). In addition, the fluorescence intensities of the different tryptophan residues in an scFv change in different directions upon unfolding: the two core Trp L43 and H43 are fully quenched in the native state, their fluorescence increases upon unfolding. In contrast, the fluorescence quantum yield of the two Trp residues H54 and H139, buried in the interface between V_L and V_H, decreases upon unfolding, reducing the net change of fluorescence intensity. The net change is thus small.

A more robust probe of the unfolding equilibrium is the wavelength of the emission maximum, λmax. Upon unfolding of the protein, the Trp side chains become more solvent exposed, and their emission spectrum is shifted towards longer wavelengths, typically from around 336 nm for a mostly buried Trp to around 350 nm for a fully solvent exposed Trp. However, due to the different fluorescence quantum yield of the native and the unfolded state, λmax is not directly proportional to the ratio of the concentrations of the unfolded and the native species. Monsellier and Bedouelle (2005) derived a correction factor to compensate for this deviation, based on the ratio of the curvatures of the spectra of the native (b(n)) and the denatured (b(u)) protein at their respective λmax (Figure S4, Table ST2). If $\Delta G'_{(H2O)}$ is the

value obtained from a two-state fit of λmax as a function of denaturant concentration (Figure S5, Table ST3), a better value of the actual $\Delta G_{(H2O)}$ is obtained by introducing the correction:

$$\Delta G_{(H2O)} = \Delta G'_{(H2O)} - RT \cdot \ln (b(n)/b(u))$$

However, comparing the magnitude of the correction terms (0.3-0.4kcal/mol, Table ST4) to the error range of the parameters of the two-state fit, the correction terms does not make a significant change to the result.

More importantly, we conclude that at least 2 of the 3 constructs do not behave as two-state systems in unfolding. The plots of λmax as a function of denaturant concentration show a marked difference in the slope of the unfolding curves for the different scFv constructs (Figure S5). This indicates that the assumption of a two-state equilibrium of unfolding is wrong. The low m-values derived from the two-state fit for constructs 4G7-wt and 4G7-mut confirm the presence of a hidden intermediate in the unfolding process. While other factors than a hidden intermediate can account for minor differences between the m-values of closely related proteins, they cannot explain the large differences observed between the m-values of 4G7-wt (2.1-3.5 kcal·L/mol^2) or 4G7-graft (2.3-2.7 kcal·L/mol^2) and of 4G7-mut (5.3-6.9 kcal·L/mol^2). The evidence for the presence of a hidden intermediate and the arguments against alternative explanations (such as e.g. incomplete denaturation at high denaturant concentration) are discussed in the accompanying paper (Honegger *et al.*, 2008) and the Supplemental Materials to that paper available at PEDS online. In addition, the very similar thermal and functional stabilities in native buffer of the three constructs investigated here are not compatible with the large difference in $\Delta G_{(H2O)}$-values derived from a two-state fit.

References

Al-Lazikani B., Lesk A.M. and Chothia C. (1997) *J. Mol. Biol.*, **273**, 927-948

Chothia C. and Lesk A.M. (1987) *J. Mol. Biol.*, **196**, 901-917

Honegger A. (2008) Engineering Antibodies for Stability and Efficient Folding. In Chernajovsky Y. and A. N. (eds) *Therapeutic Antibodies*. Springer-Verlag, Berlin-Heidelberg, pp. 47-68.

Honegger A., Malebranche A.D., Röthlisberger D. and Plückthun A. (2008) *Protein Eng. Des. Sel.*, in press, accompanying manuscript.

Honegger A. and Plückthun A. (2001a) *J. Mol. Biol.*, **309**, 687-699

Honegger A. and Plückthun A. (2001b) *J. Mol. Biol.*, **309**, 657-670

Hubbard S.J. and Thornton. J.M. (1993) NACCESS. Computer Program, Department of Biochemistry and Molecular Biology, University College London.

Kabat E.A., Wu T.T., Perry H., Gottesmann K. and Foeller C. (1991) *Sequences of proteins of immunological interest*. Fifth edn., NIH Publication No. 91-3242.

Knappik A., Ge L., Honegger A., Pack P., Fischer M., Wellnhofer G., Hoess A., Wölle J., Plückthun A. and Virnekäs B. (2000) *J. Mol. Biol.*, **296**, 57-86

Lefranc M.P., Pommie C., Ruiz M., Giudicelli V., Foulquier E., Truong L., Thouvenin-Contet V. and Lefranc G. (2003) *Dev. Comp. Immunol.*, **27**, 55-77

Monsellier E. and Bedouelle H. (2005) *Prot. Eng., Des. Sel.*, **18**, 445-456

Rothe C., Urlinger S., Lohning C., Prassler J., Stark Y., Jager U., Hubner B., Bardroff M., Pradel I., Boss M. *et al.* (2008) *J. Mol. Biol.*, **376**, 1182-1200

Santoro M.M. and Bolen D.W. (1988) *Biochemistry*, **27**, 8063-8068.

Willuda J., Honegger A., Waibel R., Schubiger P.A., Stahel R., Zangemeister-Wittke U. and Plückthun A. (1999) *Cancer Res.*, **59**, 5758-5767

Figure S1

VL-Domain

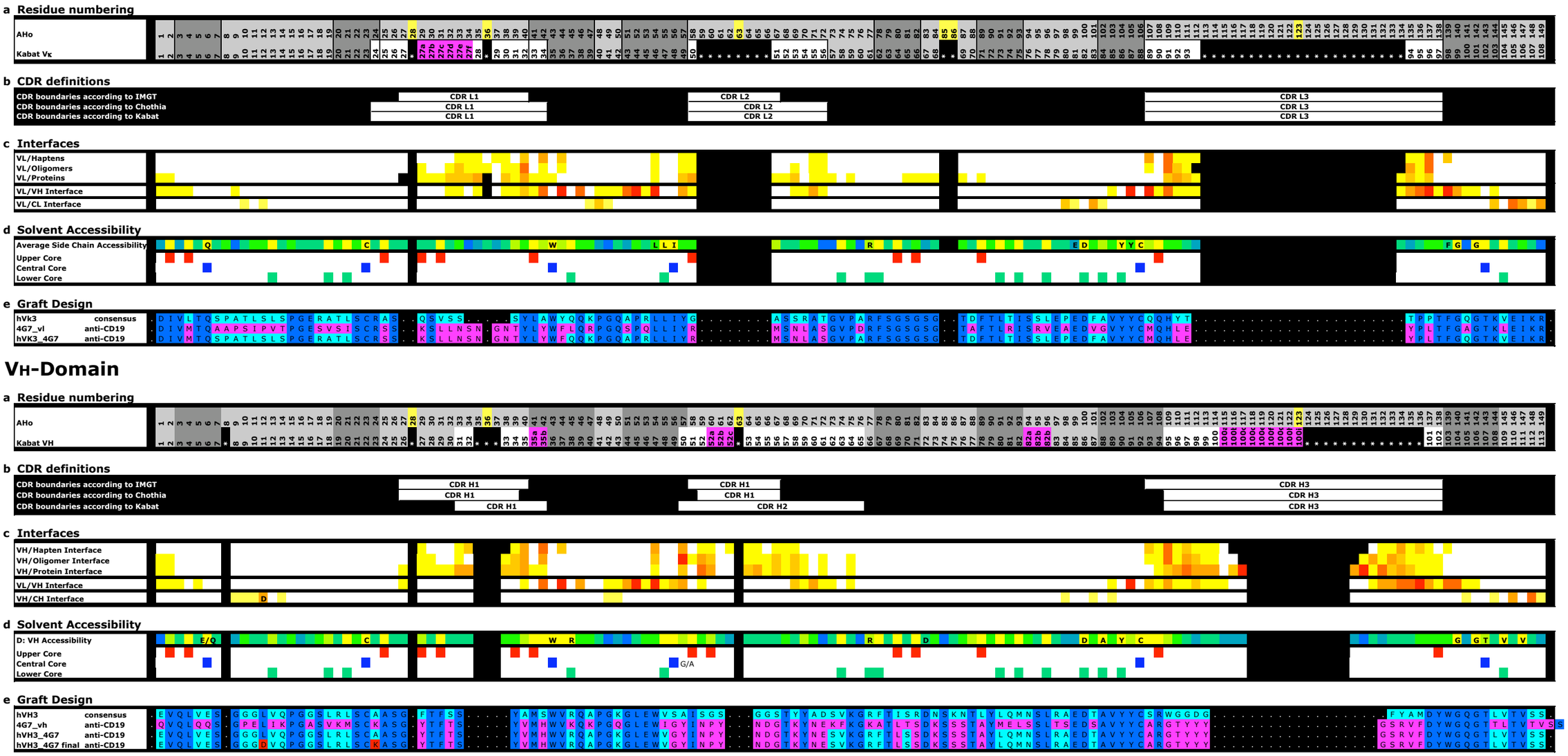

VH-Domain

Figure S1: Summary of residue information relevant to the design of a CDR graft

(a) Residue numbers according to the AHo numbering scheme (Honegger and Plückthun, 2001b) and according to the Kabat (Kabat *et al.,* 1991) numbering scheme. Gaps in the sequence alignment are to be centered on the positions highlighted in yellow to reflect the structural equivalence of the positions with the same residue number between antibodies with different CDR lengths in the AHo scheme. In the Kabat scheme, alignment gaps are accommodated in the positions marked in magenta. **(b)** CDR boundaries according to Kabat (Kabat *et al.,* 1991), Chothia (Chothia and Lesk, 1987; Al-Lazikani *et al.*, 1997) and IMGT (Lefranc *et al.,* 2003) **(c)** Comparison of the average solvent accessible surface area in the complex and in the free domains yields information on the average contribution of each residue to interface formation (white: 0% reduction, yellow: 0-20%, yellow-orange: 20-40%, orange: 40-60%, red-orange: 60-80%, red: 80-100%) for the binding of hapten antigens, linear oligomeric antigens and structural epitopes in proteins. The same analysis was performed for residues involved in V_L/V_H contacts and contact residues between the variable and constant domains. **(d)** Average relative side chain accessibility in the isolated domain: The solvent accessible surface of each residue was calculated as percentage of the solvent accessible surface the same residue would have in the context of a poly-Ala peptide in extended conformation, using the program NACCESS (Hubbard and Thornton., 1993). Numeric values were converted to a color code: yellow, 0-10% accessible, signifies a residue that is fully buried, yellow-green: 10-25%, buried; green: 25-50%, green-blue: 50-75%, semi-buried; blue: 75-100%, dark blue: >100% exposed, signifies a residue is more exposed than it would be in the context of an extended poly-Ala peptide. Fully buried (core) residues are subdivided into upper core, central core and lower core residues as described in the text. **(e)** Comparison of the sequences of the acceptor framework, the CDR donor and the graft. Residues that are identical in all three molecules are colored blue, residues that match the sequence of the acceptor framework, cyan, and residues derived from the CDR donor, magenta.

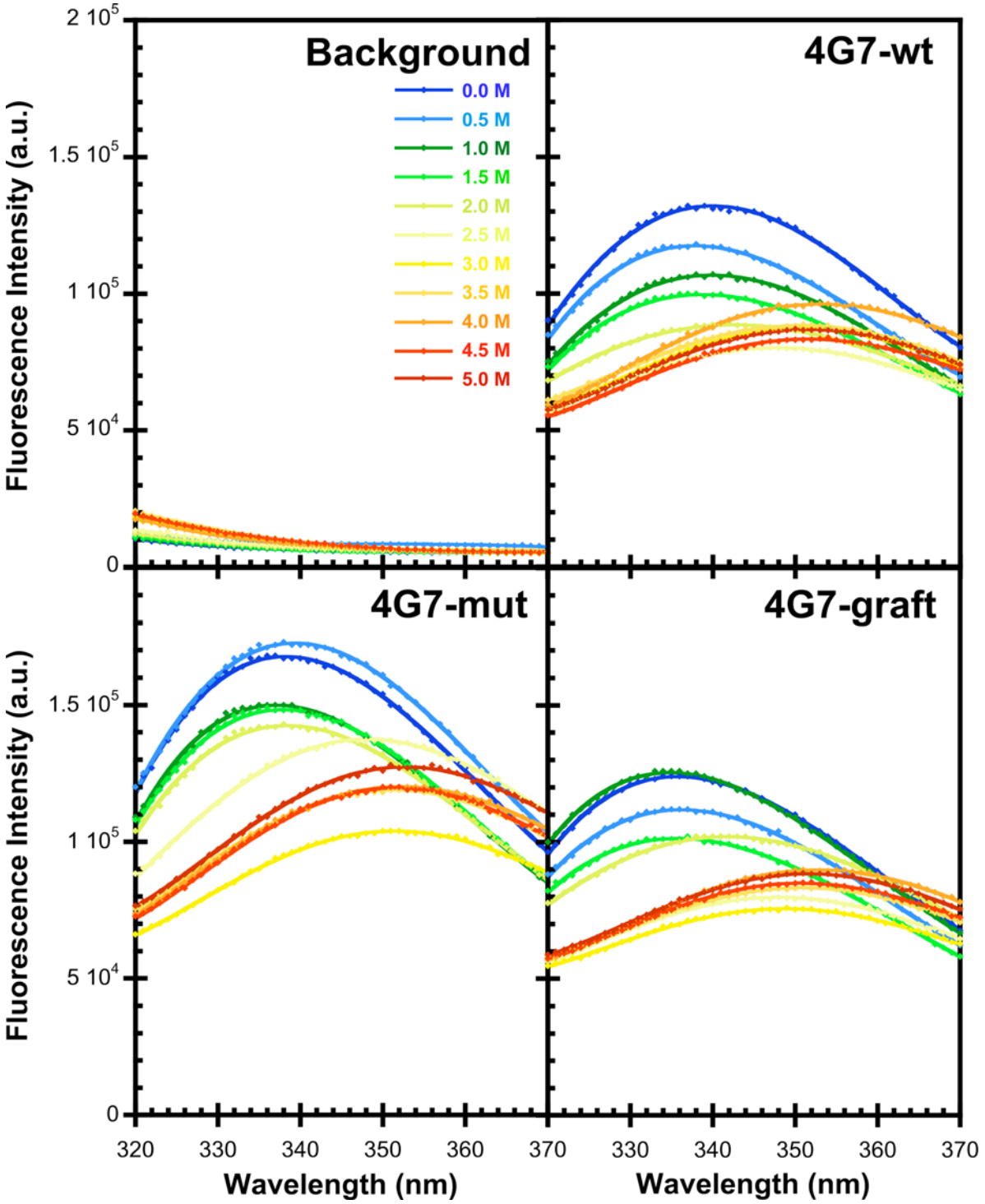

Figure S2: Trp Fluorescence spectra of the three single-chain Fv constructs in different concentrations of GdmCl. ScFv were diluted to a final concentration of 0.3 µM in 0-5 M GdmCl, 0.05 M Tris-HCl, pH 7.2 and incubated overnight at 25° C. Fluorescence spectra were recorded with an emission wavelength of 280 nm. The spectra were fitted by a Taylor series to the 4th order term as described by Monsellier and Bedouelle (2005) to determine the emission maximum, λmax.

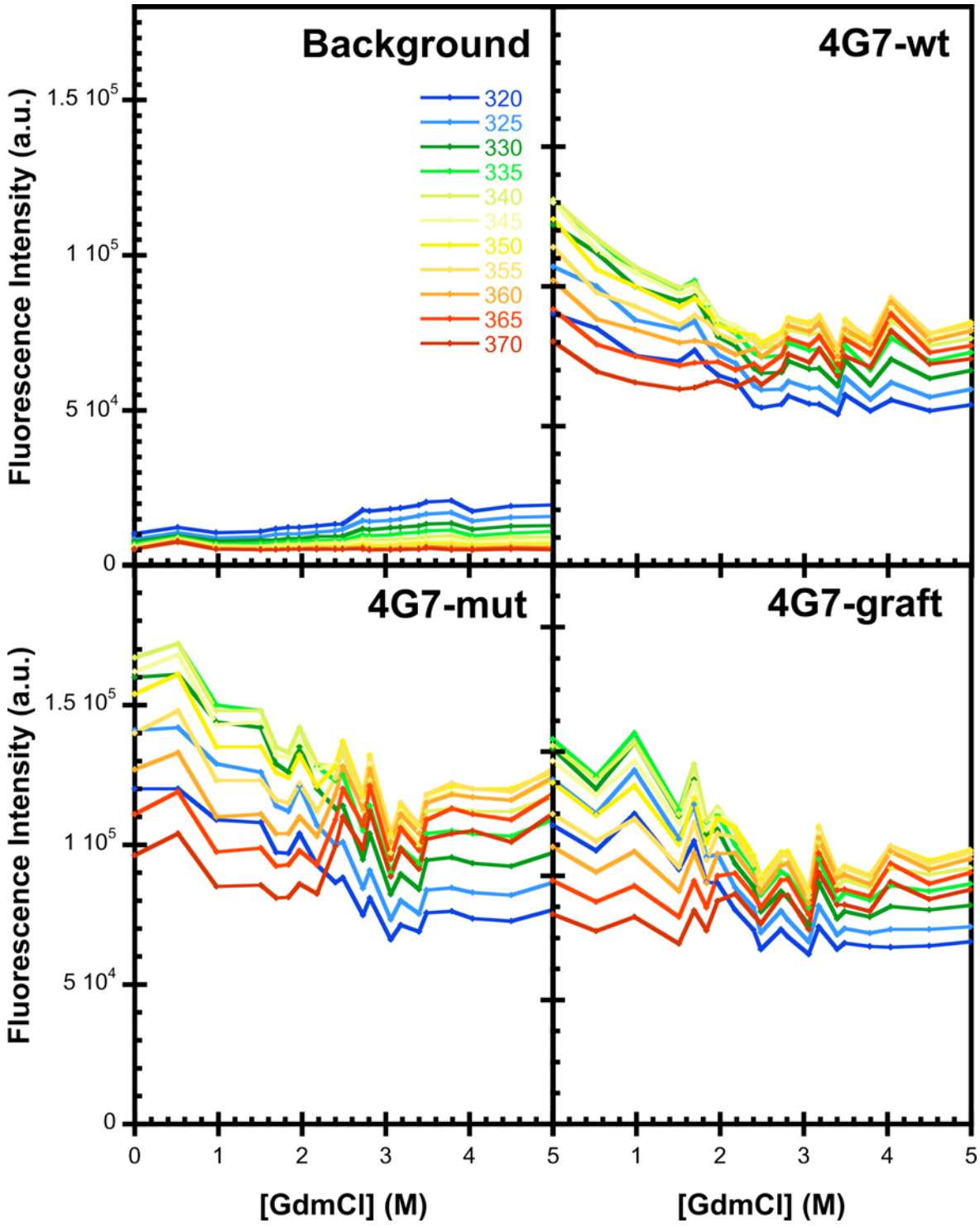

Figure S3: Plots of fluorescence intensity against guanidinium concentration. The signal-to-noise ratio is too low to derive reliable thermodynamic parameters from a two-state fit to the intensity as a function of denaturant concentration at any wavelength.

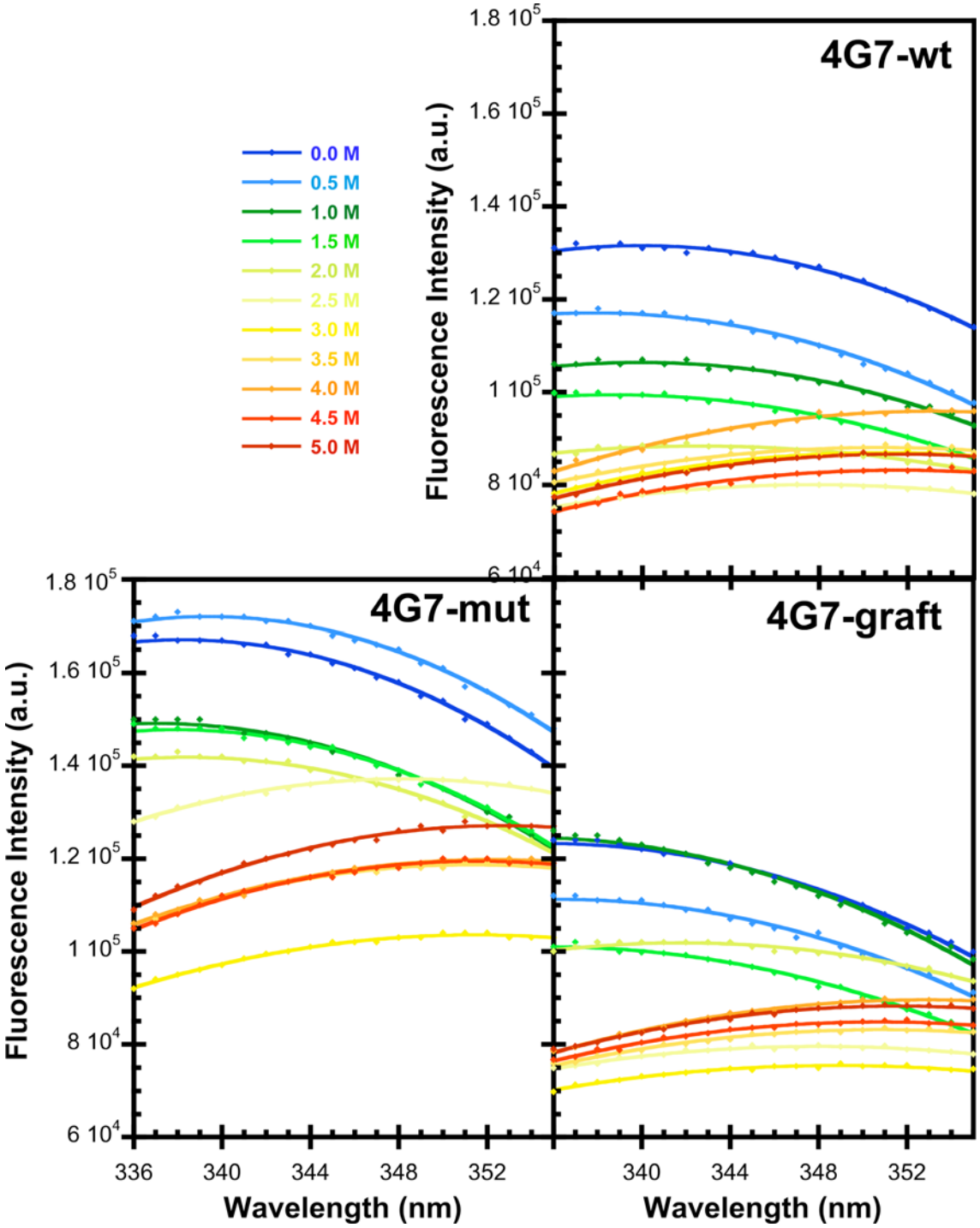

Figure S4: Curvature of the spectra at λmax

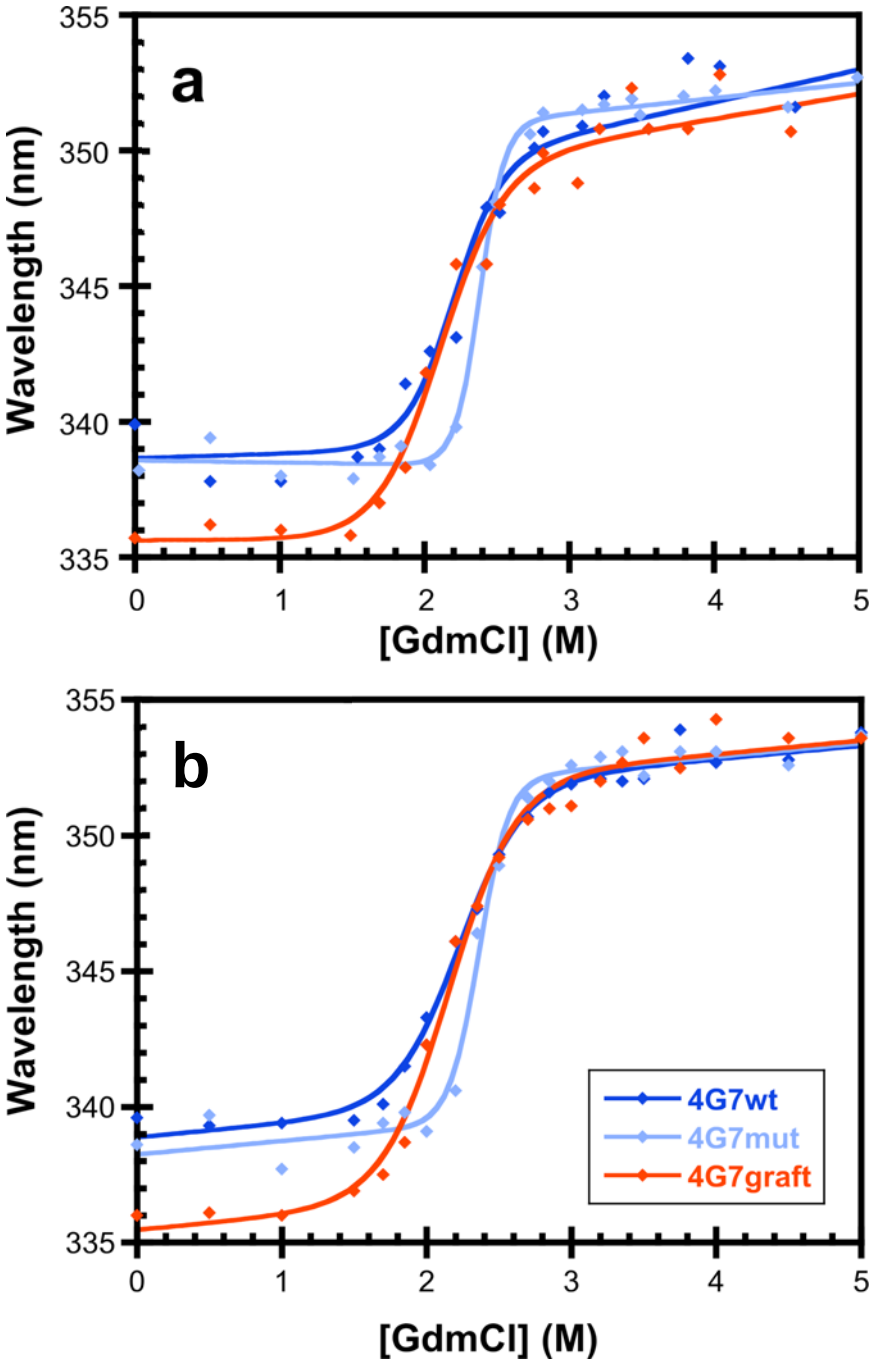

Figure S5: The wavelength of the fluorescence emission maximum plotted against guanidinium concentration for two independent experiments. The spectra were fitted by a Taylor series to the 4th order term as described by Monsellier and Bedouelle (2005) to determine the emission maximum λmax. The plots of λmax vs. [GdmCl] were fitted by a two-state model (Santoro and Bolen, 1988) (Table ST3). However, as explained above, the low m-value precludes that the system follows a two-state system, as alternative explanations can be excluded. (**a**) and (**b**) show the results of two independent experiments, using different batches of protein.

Table ST1:

Parameters derived from the fit of the function $y = m1+0.5*m2*(x-m3)^2+m4*(x-m3)^3+m5*(x-m3)^4$ to the spectra shown in Figure SX

4G7-wt	m1		m2		m3		m4		m5		R
[GdmCl](M)	Ymax		Curvature at λmax		λmax						
0.0	**1.32E+05**	± 196	**-193.2**	± 3.0	**339.9**	± 0.13	**0.94**	± 0.077	**0.013**	± 0.0035	0.9989
0.5	**1.17E+05**	± 143	**-173.2**	± 1.9	**337.8**	± 0.12	**1.21**	± 0.080	**0.002**	± 0.0026	0.9993
1.0	**1.07E+05**	± 152	**-143.2**	± 2.3	**339.9**	± 0.13	**0.71**	± 0.062	**0.006**	± 0.0027	0.9989
1.5	**99619**	± 121	**-127.4**	± 1.7	**338.7**	± 0.13	**0.84**	± 0.061	**0.001**	± 0.0022	0.9991
2.0	**88559**	± 97	**-77.4**	± 1.8	**342.6**	± 0.13	**0.19**	± 0.024	**0.005**	± 0.0016	0.9986
2.5	**80169**	± 58	**-75.4**	± 1.1	**347.7**	± 0.08	**0.07**	± 0.013	**0.011**	± 0.0010	0.9995
3.0	**87168**	± 71	**-88.1**	± 1.1	**350.9**	± 0.11	**0.03**	± 0.029	**0.014**	± 0.0013	0.9995
3.5	**88304**	± 97	**-80.7**	± 1.6	**350.8**	± 0.16	**0.02**	± 0.039	**0.012**	± 0.0017	0.9989
4.0	**96148**	± 107	**-96.3**	± 1.5	**353.1**	± 0.16	**0.10**	± 0.058	**0.016**	± 0.0019	0.9993
4.5	**83327**	± 81	**-79.5**	± 1.3	**351.6**	± 0.14	**0.10**	± 0.035	**0.014**	± 0.0015	0.9993
5.0	**86809**	± 74	**-85.9**	± 1.1	**351.6**	± 0.12	**0.04**	± 0.032	**0.015**	± 0.0013	0.9995
4G7-mut											
0.0	**1.68E+05**	± 203	**-247.4**	± 2.8	**338.2**	± 0.11	**1.60**	± 0.109	**0.002**	± 0.0037	0.9993
0.5	**1.73E+05**	± 193	**-248.3**	± 2.9	**339.4**	± 0.10	**1.32**	± 0.085	**0.011**	± 0.0034	0.9994
1.0	**1.50E+05**	± 193	**-229.9**	± 2.7	**337.0**	± 0.12	**1.85**	± 0.121	**-0.005**	± 0.0035	0.9993
1.5	**1.48E+05**	± 185	**-217.3**	± 2.5	**337.9**	± 0.12	**1.43**	± 0.103	**0.002**	± 0.0033	0.9993
2.0	**1.42E+05**	± 197	**-193.3**	± 2.7	**338.4**	± 0.14	**1.20**	± 0.102	**0.002**	± 0.0035	0.9990
2.5	**1.38E+05**	± 153	**-142.7**	± 2.9	**348.1**	± 0.11	**0.27**	± 0.039	**0.019**	± 0.0026	0.9992
3.0	**1.04E+05**	± 103	**-105.9**	± 1.6	**351.5**	± 0.13	**0.13**	± 0.044	**0.019**	± 0.0018	0.9994
3.5	**1.19E+05**	± 115	**-118.3**	± 1.8	**351.3**	± 0.13	**0.17**	± 0.049	**0.020**	± 0.0021	0.9994
4.0	**1.20E+05**	± 112	**-115.1**	± 1.7	**352.2**	± 0.14	**0.18**	± 0.056	**0.017**	± 0.0020	0.9995
4.5	**1.20E+05**	± 125	**-129.1**	± 2.0	**351.6**	± 0.13	**0.21**	± 0.055	**0.024**	± 0.0022	0.9994
5.0	**1.27E+05**	± 130	**-132.6**	± 1.9	**352.7**	± 0.14	**0.19**	± 0.067	**0.023**	± 0.0023	0.9995
4G7-graft											
0.0	**1.24E+05**	± 101	**-182.4**	± 1.5	**335.7**	± 0.08	**1.43**	± 0.071	**-0.005**	± 0.0018	0.9997
0.5	**1.12E+05**	± 120	**-155.7**	± 1.7	**336.2**	± 0.11	**1.00**	± 0.080	**0.001**	± 0.0021	0.9995
1.0	**1.25E+05**	± 123	**-190.1**	± 2.1	**334.8**	± 0.09	**1.54**	± 0.092	**-0.005**	± 0.0021	0.9997
1.5	**1.01E+05**	± 118	**-130.3**	± 1.7	**335.8**	± 0.13	**0.89**	± 0.082	**-0.002**	± 0.0021	0.9994
2.0	**1.02E+05**	± 103	**-103.2**	± 1.8	**341.8**	± 0.11	**0.24**	± 0.028	**0.009**	± 0.0018	0.9991
2.5	**79772**	± 91	**-76.8**	± 1.7	**348.0**	± 0.12	**0.07**	± 0.022	**0.012**	± 0.0016	0.9988
3.0	**75617**	± 84	**-71.8**	± 1.5	**348.8**	± 0.13	**0.05**	± 0.022	**0.014**	± 0.0015	0.9987
3.5	**83296**	± 77	**-77.6**	± 1.2	**350.8**	± 0.13	**0.02**	± 0.030	**0.013**	± 0.0014	0.9992
4.0	**89787**	± 78	**-88.4**	± 1.1	**352.8**	± 0.13	**0.07**	± 0.040	**0.015**	± 0.0014	0.9995
4.5	**84965**	± 75	**-84.2**	± 1.2	**350.7**	± 0.12	**0.11**	± 0.028	**0.017**	± 0.0013	0.9994
5.0	**88392**	± 70	**-89.7**	± 1.1	**351.6**	± 0.11	**0.04**	± 0.031	**0.017**	± 0.0013	0.9995

Table ST2: Curvatures at λmax as a function of guanidinium concentration for the spectra shown in Figures S2 and S4

4G7-wt		m1		m2	
[GdmCl](M)	λmax	Ymax		Curvature at λmax	R
0.0	**339.9**	**1.32E+05** ± 164		**-155.4** ± 3.42	0.996
0.5	**337.8**	**1.17E+05** ± 168		**-133.8** ± 2.55	0.997
1.0	**339.9**	**1.06E+05** ± 175		**-118.9** ± 3.64	0.992
1.5	**338.7**	**9.94E+04** ± 137		**-102.9** ± 2.38	0.995
2.0	**342.6**	**8.84E+04** ± 110		**-69.0** ± 3.59	0.977
2.5	**347.7**	**8.01E+04** ± 65		**-70.9** ± 2.37	0.990
3.0	**350.9**	**8.70E+04** ± 88		**-78.9** ± 1.89	0.995
3.5	**350.8**	**8.81E+04** ± 111		**-69.0** ± 2.43	0.989
4.0	**353.1**	**9.59E+04** ± 134		**-88.6** ± 2.06	0.995
4.5	**351.6**	**8.32E+04** ± 119		**-73.2** ± 2.29	0.991
5.0	**351.6**	**86647** ± 76		**-78.1** ± 1.46	0.997
4G7-mut					
0.0	**338.2**	**1.67E+05** ± 198		**-195.0** ± 3.18	0.998
0.5	**339.4**	**1.72E+05** ± 185		**-202.9** ± 3.56	0.997
1.0	**337.0**	**1.49E+05** ± 251		**-166.4** ± 3.41	0.996
1.5	**337.9**	**1.48E+05** ± 200		**-171.8** ± 3.08	0.997
2.0	**338.4**	**1.42E+05** ± 202		**-149.5** ± 3.35	0.996
2.5	**348.1**	**1.37E+05** ± 114		**-126.5** ± 3.91	0.991
3.0	**351.5**	**1.04E+05** ± 100		**-94.6** ± 1.95	0.996
3.5	**351.3**	**1.19E+05** ± 123		**-109.0** ± 2.49	0.995
4.0	**352.2**	**1.20E+05** ± 143		**-106.3** ± 2.51	0.995
4.5	**351.6**	**1.19E+05** ± 141		**-121.1** ± 2.71	0.996
5.0	**352.7**	**1.27E+05** ± 162		**-126.0** ± 2.64	0.996
4G7-graft					
0.0	**335.7**	**1.23E+05** ± 243		**-131.1** ± 2.79	0.996
0.5	**336.2**	**1.11E+05** ± 218		**-118.5** ± 2.67	0.995
1.0	**334.8**	**1.25E+05** ± 311		**-134.4** ± 3.20	0.995
1.5	**335.8**	**1.01E+05** ± 191		**-101.3** ± 2.23	0.996
2.0	**341.8**	**1.02E+05** ± 133		**-95.5** ± 3.79	0.986
2.5	**348.0**	**7.96E+04** ± 91		**-67.1** ± 3.17	0.981
3.0	**348.8**	**7.55E+04** ± 89		**-64.1** ± 2.73	0.984
3.5	**350.8**	**8.32E+04** ± 102		**-70.9** ± 2.23	0.991
4.0	**352.8**	**89592** ± 83		**-80.7** ± 1.33	0.998
4.5	**350.7**	**84838** ± 91		**-77.9** ± 2.02	0.994
5.0	**351.6**	**88255** ± 103		**-82.2** ± 1.98	0.995

Table ST3: Thermodynamic parameters derived from a two-state fit

	ΔG(H2O)			m			[D]50			R	Mpred[2]
a	kcal/mol			kcal*L/mol^2			mol/L				kcal*L/mol^2
4G7wt	**4.7**	±	0.50	**2.1**	±	0.21	**2.2**	±	0.29	0.991	**5.6**
4G7mut	**12.5**	±	0.81	**5.3**	±	0.34	**2.4**	±	0.47	0.997	**5.9**
4G7graft	**4.7**	±	0.36	**2.3**	±	0.16	**2.1**	±	0.20	0.996	**5.9**
huVκ3-huVH3[1]	**7.0**	±	0.33	**2.7**	±	0.13	**2.6**	±	0.20	0.999	**5.9**
b											
4G7wt	**5.9**	±	0.61	**2.6**	±	0.3	**2.2**		0.3	0.997	
4G7mut	**13.5**	±	2.49	**5.7**	±	1.1	**2.4**		1.4	0.996	
4G7graft	**5.5**	±	0.60	**2.5**	±	0.3	**2.2**		0.3	0.996	
huVκ3-huVH3[1]	**6.9**	±	0.03	**2.7**	±	0.0	**2.6**		0.0	0.999	
c											
4G7wt	**7.7**	±	3.16	3.5	±	1.4	2.2		1.8	0.985	
4G7mut	**16.4**	±	2.85	6.9	±	1.2	2.4		1.7	0.998	
4G7graft	**5.6**	±	1.14	2.7	±	0.6	2.1		0.6	0.990	
huVκ3-huVH3[1]	**6.9**	±	0.04	2.6	±	0.0	2.6		0.0	0.999	

(a) Parameter derived if a two-state model is applied to the data shown in Figure 5 of the paper, based on λmax values determined by a Gaussian fit to the spectra

(b,c) Parameter derived from the data shown in Figure S4 (a) and (b). Two independent unfolding curves were measured with different batches of protein. In these experiments, λmax was determined by fitting a Taylor series to the 4th order term to the spectra as described by Monsellier and Bedouelle (2005)

[1] from Honegger *et al.*, (2008)

[2] calculated according to Myers *et al.*, (1995).

Table ST4: Correction factors

	b(n)	b(u)	b(n)/b(u)	RT* ln (b(n)/b(u)) kcal/mol
4G7-wt	-155.4	-78.1	1.99	**0.41**
4G7-mut	-195.0	-126.0	1.55	**0.26**
4G7-graft	-131.1	-82.2	1.59	**0.28**